J. Condensed Matter Nucl. Sci. 15 (2015) 55–65

Research Article

Conservation of E and M, Single Cavitation Heat Events

Roger S. Stringham*

First Gate Energies, P.O. Box 1230, Kilauea, HI 96754, USA

Abstract

Experiments spread over a period of 24 years create a model for sonofusion. An explanation of results will influence new paths for its further development. Cavitation produced z-pinch target-foil implanting jets produce SEM photos of single event ejecta sites equal to the binding energy differences, E_b, for alpha production.
 ISSN 2227-3123

Keywords: Alpha, Cavitation, Jets, Photons

1. Introduction

The initial D_2O cavitation work started in March of 1989 with a 20 kHz resonator adapted from Heat Systems Inc., and resulted in a melted and discolored Pd target foil. In 1993, work with Ti target foils in 46 kHz systems produced a standing wave of 2.3 mm λs approximating the 1.6 MHz frequency that was adopted in 2003 and has been in use since.

In measured systems, calorimetric data corresponds with survey counts of ejecta site craters, ejs, in scanning electron microscope, SEM, photos of target foils. SEM photos at three frequencies of exposed targets were especially compelling. Figure 1a (2003) shows a newer Pd foil exposed at 1.6 MHz with single event ejs of E_b, Eq. (1) [1,2], where ejs debris is expelled with velocity and mass of 20 $\pm$10 MeV. Figure 1b (1993) shows a Pd foil exposed at 46 kHz, with multiple 23.8 MeV, E_b, events 1993 [1], Figure 1c shows the standing wave on a Ti foil and the associated nodal lines of E_b distribution 1993 [2,3]. Surveys of target foils indicated a strong correlation between the size and number of ejecta sites and the excess heat generated, with the estimated energy of 20 $\pm$10 MeV, close to the binding energy difference, E_b, of $2D^+ \rightarrow \alpha$, Eq. (1).

$$B(2D^+;\alpha) = B - (2p, 2n;\alpha) - 2B(p, n; D^+) = 28.3 - 2 \times 2.25 = 23.8\ \text{MeV} = E_b. \quad (1)$$

This indicated an event occurring at time $t' = 0$, during a picosecond timeframe, in which a dense deuteron condensate, $M = nD^+$, becomes a two particle system, α and M', where M' is an expanding center of mass (COM)

*E-mail: firstgate@earthlink.net

 ISSN 2227-3123

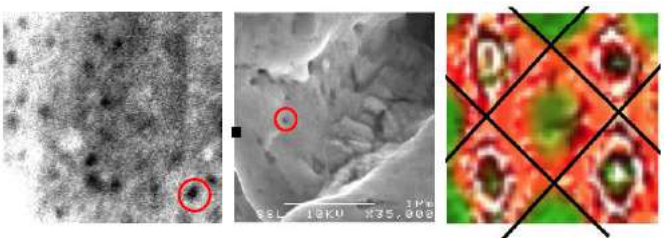

Figure 1. (a) Left :Pd foil, 1.6 MHz 1 μm^2. (b) Middle: Pd foil, 46 kHz 2 μm^2. (c) Right: TiOx nodal lines 46 kHz, .33 cm^2.

of residual deuterons, Eq. (2).

$$M \rightarrow M' + \alpha + E_{\mathrm{b}}/c^2 \text{ kg mass}; M' = M - 2\mathrm{D}^+, \tag{2}$$

While ^{4}He measurements of early kHz systems influenced development of the model, most of the data in this paper comes from the more recent 1.6 MHz system, Fig. 1a. Section 2 describes the experimental design used to collect flow-through calorimetry data. Section 3 presents the data that provides a basis for the model in Section 4, which complies with the laws of conservation of energy and momentum.

2. Experimental Design

The polycarbonate resonator was divided into three parts. "A" is the cap, which serves as a window and seals "B" enclosing the resonant volume, including a 1 g/s D_2O flow, a target foil, a calibration heater, a piezo-electric transducer, and a seal to "C". "C" allows for the Ar pressure balance for "B" and across the piezo thickness to "C", where the oscillator's electric connections for acoustic input, Q_{a}, are made, Fig. 2.

The power supply to the oscillator, Q_i, was connected into the 120 V 60 cycle utility. The D_2O had a residence time of 0.5 s in the 0.5 cm^3 volume resonator. Connections for the 12 W resistance calibration heater are within the resonator volume. The target foil was configured to be 1 mm from the 1.6 MHz PZT piezo disk (2 mm thick and 10 mm radius). The circulating system was on a duty cycle of 120 s off and on. Duty cycles of 60–200 s were also used. The temperature data was taken each second, and measurements were made at the beginning of the off-mode and extrapolated back to the last point of the on-mode. This process avoided a potential radio frequency interference of thermocouple ΔT data from the 1.6 MHz Q_{a} oscillator.

A D_2O flow system, Fig. 3, circulated D_2O at 1 g/s with an FMI constant mass-flow pump measured by the flow meter. D_2O passes through a filter, proceeding to a light box that contains a resonator, target foil, calibration heater, and a variable Q_{a} oscillator input. In the resonator are thermocouples measuring T in and out, ΔT. Photomultipliers and multipixel photon counters (MPPC) from Hamamatsu measured photon emission (PE) that is the sum of sono-luminescence (SL) of collapsing bubbles, as well as any non-absorbed Bremsstrahlung (Br) photons [2]. The flow continues to a flow-meter, a heat exchange coil, and a bubbler. The bubbler, connected to a vacuum line, controls the pressurized Ar gas saturating 20 ml of circulating D_2O and a gas sampling valve system. The bubbler separates any in-line circulation bubbles and has a direct connection back to the FMI pump completing the D_2O cycle.

3. Data Collection

Calorimetric data, supported by calibration heater Figs. 2 and 3, of the 1.6 MHz systems showed excess heat, Q_x, generated relative to acoustic input, Q_{a}. Surveys of SEM images of exposed target foils indicated 10^7 events/cycle,

each producing $E_{\rm b}$, the sum corresponding to measured Q_x. Also relevant to the model, intermittent ^{4}He mass spectrum, MS, measurements from the early 20 kHz systems showed some correspondence to Q_x and suggested inefficient cavitation. The introduction of multipixel photon counting, MPPC, Hamamatsu technology allowed for the use of PE signals as feedback for adjusting $Q_{\rm a}$ input to produce efficient cavitation. MPPC data shows an active zone of 100 ns, establishing a basis for a model timeline.

3.1. Some calorimetric data

Figure 4 shows flow-through calorimetry data from a 20 g 1.6 MHz resonator, which was used many times to generate data. The table in the upper right lists, in chronological order, a series of 10 data points at 1 atm. of Ar saturated D_2O circulating at 60 g/min. The data was produced by varying the input Q_i, where the oscillator's acoustic input, $Q_{\rm a} = .3Q_i$, thus changing the total heat output, $Q_{\rm o}$, and excess heat, Q_x. The numerical values were collected for $Q_{\rm a}$, $Q_{\rm o}$, and Q_x were measured at 1 s intervals.

$$Q_{\rm o} - Q_{\rm a} = Q_x \text{ and } Q_{\rm a} = .3Q_i. \tag{3}$$

The D_2O rate of mass flow, F, through the resonator multiplied by ΔT was used to calculate the calorimetric $Q_{\rm o}$ measured heat as $\Delta T \times F$ calories [1,2]. Figure 4 plots showes a tipical result. The system, running at maximum $Q_{\rm a}$,

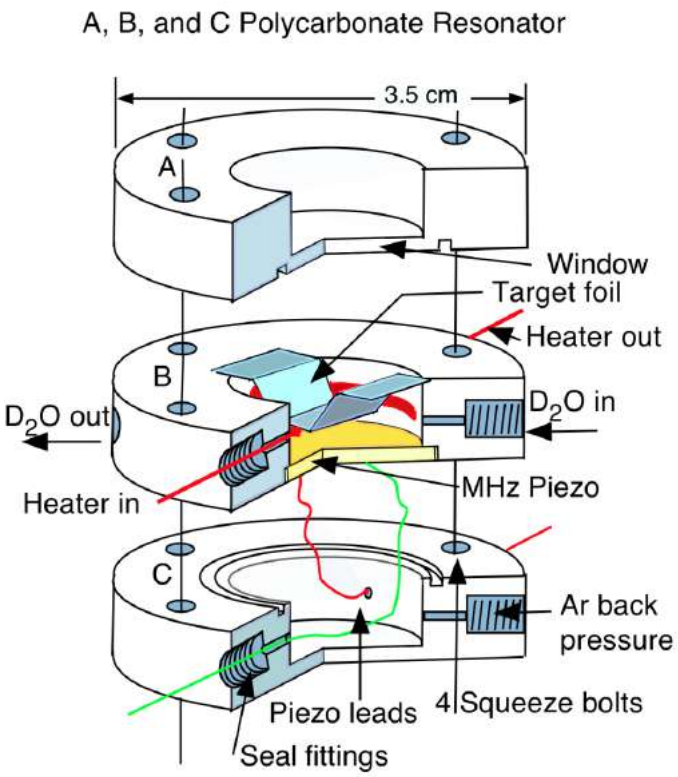

Figure 2. One view of a three-piece polycarbonate piezo resonator.

was at also at maximum Q_x for pressure, temperature, Q_a, and PE that were the controlling parameters. The data also shows straight line increase of Q_x vs Q_o and Q_a W, linking PE increases [4], see Fig. 5. The measured ΔT°C was used to calculate Q_o, and a watt-meter Q_a, see Fig. 3 [2].

3.2. SEM images

The removal of the exposed 100 μm thick Pd target foils from the 1.6 MHz resonator allowed for a leisurely SEM analysis of the craters, ejecta sites, on its surface. The red circles in Fig. 1a,b highlight 50 nm ejecta sites, corresponding to single events and occurring in both the older 46 kHz and newer 1.6 MHz resonators [1,2]. Figure 1a shows the uniformity of 50 nm ejecta sites in the 1.6 MHz resonator, in contrast with range of sizes indicating mostly multiple with single events in the older 46 and 20 kHz resonators [1]. Figure 1c shows the standing wave nodal plane of a Ti target foil surface exposed at 46 kHz, with ejecta sites distributed along the nodal lines as indicated [3]. Additional

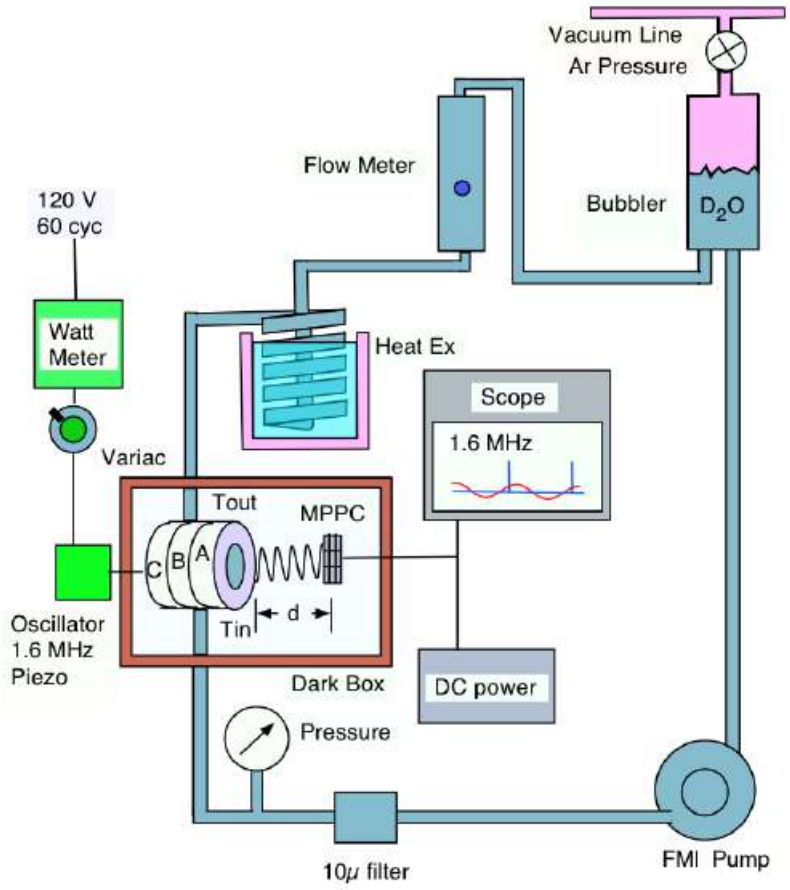

Figure 3. Flow system of D_2O through the resonator.

photos and videos are in possession of the author, showing slight to catastrophic foil damage depending on the thickness, element composition, and resonant frequency and amplitude of Q_a [1,3].

The 1.6 MHz single event ejecta sites were observed and counted in an area of 1 μm^2, Fig. 1a. The ejecta site count was extrapolated to its nodal plane area, which was one-hundredth of the 1 cm^2 target foil. The number of ejecta sites for one cycle was estimated at 10^7, each producing E_b, 23.8 MeV or 3.82×10^{-12} J. These numbers support 38 W of Q_x production at a 15 W Q_a input [5]. These photos and the calorimetry data support the occurrence of target foil events 25 nm below the foil surface, ejecting from the surface in expanding spherical heat pulses, E_b/s = Q_x [1].

3.3. The helium measurement

Helium measurements for early kHz cavitation systems were carried out in three laboratories: in 1991, by Dave Thomas at Stanford Research Institute (SRI); in 1992–1993 by Dr. Davidson of the US Bureau of Mines in Amarillo, TX; and in 1994-5, samples taken at Los Alamos National Laboratory (LANL) were analyzed by Brian Oliver at the Department of Energy, DOE, facility at Rocketdyne, CA. Brian Oliver also used MS measurements to track a sample of Ti target foil gases that change over time, showing decay of T to ^{3}He at the rate of the disintegration constants confirming the origin of the growing ^{3}He [3]. The Appendix at the end of this paper provides details on these measurements .

Reproducibility in He measurements suggested inefficient cavitation due to small variations in temperature, pressure, and acoustic input parameters. Thus, subsequent versions of resonators introduced the MPPC, new technology from Hamamatsu, which measures PE and couples it with significant changes to the MHz acoustic input, Q_a, suppressing small effects in resonator's T and P. This innovation in the MHz system produced better photon cavitation tracking. The MHz calorimetry, with no costly He measurements, was the basis for the Q_x determination.

3.4. SL and Br photon emission data

Figure 5 shows a typical 10,000 ns of MPPC data set at the following conditions: distance (d) of 8–16 cm from resonator to MPPC with a Q_a = 4.2 W. The PE signal, in blue, is coupled with the acoustic Q_a pulse, in red. PE is

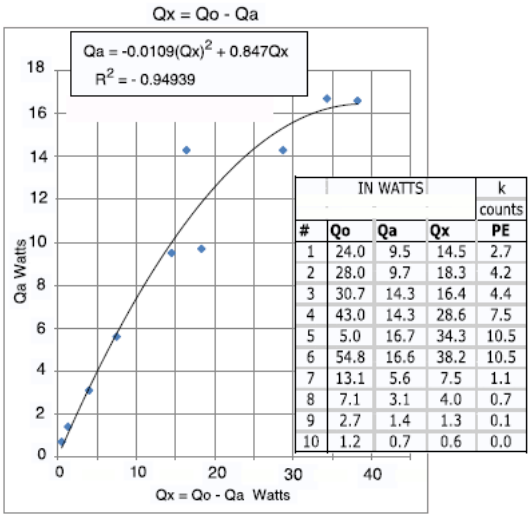

	IN WATTS			k counts
#	Qo	Qa	Qx	PE
1	24.0	9.5	14.5	2.7
2	28.0	9.7	18.3	4.2
3	30.7	14.3	16.4	4.4
4	43.0	14.3	28.6	7.5
5	5.0	16.7	34.3	10.5
6	54.8	16.6	38.2	10.5
7	13.1	5.6	7.5	1.1
8	7.1	3.1	4.0	0.7
9	2.7	1.4	1.3	0.1
10	1.2	0.7	0.6	0.0

Figure 4. The relation between Q_o, Q_a, Q_x, and PE (photon emission).

produced by the SL of 10^6 collapsing bubbles and as Br photons not absorbed as heat during the distribution of E_b. Some unabsorbed Br photons degraded to low energies, and pass through to MPPC, registering in the PE measurement. The sum of Br photons less than .01% of Q_x, Fig. 5.

The MPPC's 1 mm^2 sensing area measures an average of 10^9 photons over time intervals of 100 ns, occupying less than 10% of each acoustic cycle [5]. This suggests future work could reduce the period of non-activity, perhaps by applying higher frequencies. The model in Section 4 describes the events in this 100 ns of activity zone, from the time the bubbles collapse through Q_x generation. This event sequence for α production will be shown to comply with the conservation of energy and momentum.

4. The Model: Timeline 100 ns

4.1. The cavitation bubble

A 20–50 g resonator via an oscillator driven piezo-electric transducer produces MHz cavitation bubbles in the flow of Ar saturated D_2O. From the spectrum of generated bubble sizes, only those bubbles that match physical size, pressure, temperature, and frequency will resonate [6]. The bubbles in resonance rapidly grow isothermally, increasing in mass and size to maximum radius R_o [1]. While in the acoustic positive phase the bubble adiabatically collapses in a few ns to the final bubble radius, R_f. Bubbles respond to the magnitude of the Q_a pressure wave. Bubbles of resonant size will oscillate in the acoustic field for millions of cycles, when Q_a is a few tenths of an atmosphere. Increasing Q_a to several atmospheres, the bubble will collapse in a single acoustic cycle. Its surface will accelerate toward its center at Mach 10 velocity [7], releasing SL and a z-pinch jet, with target foil implant ns later.

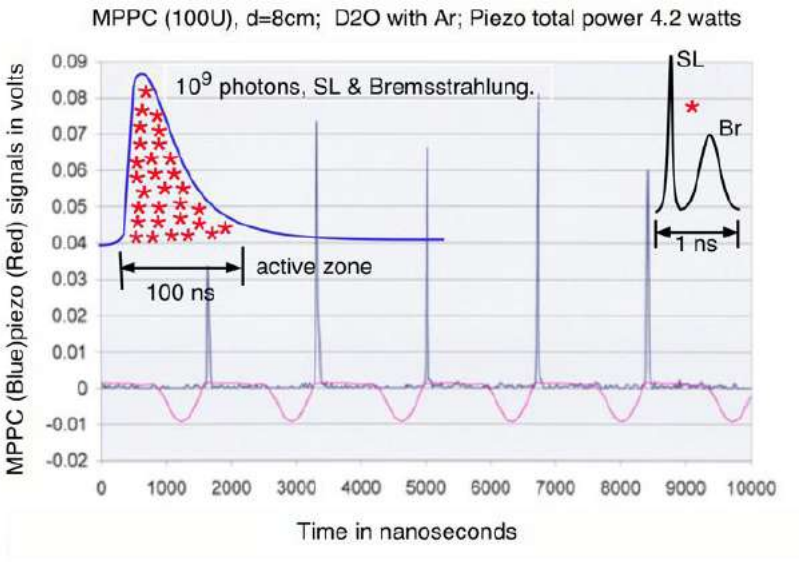

Figure 5. The 100 ns MPPC signal is the coupled activity zone. The inset, upper right, looks at a 1 ns speculated PE of SL and Br for one bubble, before photon absorption by the polycarbonate resonator's 350 nm cut-off. A major part of the sequence producing *M* clusters.

4.2. The z-pinch jet

The plasma contents of the bubble have become rearranged such that a high density deuteron plasma is confined and compressed by the electromagnetic pressure of a sheath of electrons carried over from the bubble's interface. The jet's velocity will be higher than the bubble's interface velocity of Mach 10 [7]. An encircling and squeezing B field further compresses the jet, narrowing its radius and further accelerating the jet's sheath electrons [8]. In the absence of intervention, this pressure will narrow the jet's radius until it disintegrates entirely, an effect that has frustrated Tokamak type research directions. In sonofusion systems, z-pinch provides an initial compression of the deuteron plasma, which is then implanted in a Pd target lattice before z-pinch collapses the jet.

When the jet implants the lattice, the much larger Ar^{+} and O^{-2} ions are held at the surface. In fact, Figure 1c shows the iridescent TiOx films, which EDS and EDX measurements found to be of varying thicknesses [4].

4.3. The *M* condensate

When the z-pinch jet implants the lattice, the outside sheath electrons of the z-pinch jet are implanted first as a highly mobile free electron cloud, followed by the equally small but more massive and less mobile deuterons. Each implantation captures a number, n, of deuterons in a dense compressing condensate, $M = n\mathrm{D}^{+}$. Each z-pinch jet implant or viable bubble produces a number of M condensates that varies from 2 to 100, for a total of 10^{7} M clusters from 10^{6} viable bubbles, 10^{13} clusters/s [9]. This implantation process produces a charge separation of picosecond duration between the *M* condensate and its surrounding electron cloud.

4.4. Image charge pressure

Lawandy [9] shows that like charged particles will attract via an image charge under rare conditions: at separations, d, below 10^{-10} m; and between interface boundaries with permittivity differences of 1000. Image charge refers to the attractive force between one particle and its similarly charged neighbor's image, reflected on the opposing side of an interface. The extreme picosecond densities of free electrons form boson charged particles, Cooper Pairs, CP, that work together to squeeze M.

The permittivity factor β across the interface is calculated with the formula in Fig. 6, and must be between –0.5 and –1 for image forces to be effective. With a mass 1800 times that of its surrounding CP electrons, the M condensate of D^{+} has a corresponding difference in relative mobility, so the permittivity factor β between the M condensate and its surrounding CP electrons approaches the –1 limit [9,10].

Having satisfied these rare conditions, CP with like charges have energies of attraction across a mutual phase boundary, the interface in Fig. 6, via an image charge of –2. The interface distance to its image charge was d and to its image in M was also d for a total of $2d$, see Fig. 6 right corner, where the immediate Pd is in a plasma state. M is in compression as x shrinks and squeezes the M interface. The shrinking triangle formed by $2d$, S, and x produce this pressure as a spherical compression piston [7].

4.5. The picosecond EM pulse

The magnetic field B runs parallel to the spherical interface of the M condensate and perpendicular to the attractive force, further containing M. This magnetic field together with the centrally focused electric field produces a picosecond electromagnetic pulse that compresses M. Deuteron separation becomes less than that of muon fusion, leading directly to the moment of event formation at $t' = 0$. This produces a 2-particle system of M' and α, with their respective energy and momentum, dispersing E_{b}/s of 23.8 MeV/s into the lattice and the circulating D_2O.

4.6. Conservation of energy and momentum

The picosecond squeeze of the M condensate results in Eq. (2) at t' = 0, where heat is transported to the circulating D_2O by two particles, α and M', both originating in M. In a classical system, during the compression of M, its center is considered stationary. At $t' = 0$, M' rapidly expands with its center of mass, COM, momentum opposed to the connected α momentum, with a sum of 0. Equations for conservation of energy (4) and momentum (5) yield non-relativistic calculations for $v_{M'}$ and v_α, with E_b = 23.8 MeV and m_α at 6.64477×10^{-27} kg.

$$E_b = .5(m_{M'}v_{M'}^2 + m_\alpha v_\alpha^2), \tag{4}$$

$$0 = m_{M'}v_{M'} - m_\alpha v_\alpha. \tag{5}$$

Table 1 gives m_M', v_M' , and v_α for M' = 98 D^+, 38 D^+, 18 D^+, 4 D^+, and 0 D^+.

The last line of this table, M' = 0 D^+, requires a relativistic calculation. It is included here to show that the lower limit produces results approaching muon fusion. Figure 7 illustrates the conservation of energy and momentum for different sizes of M condensates, including the lower kg limit.

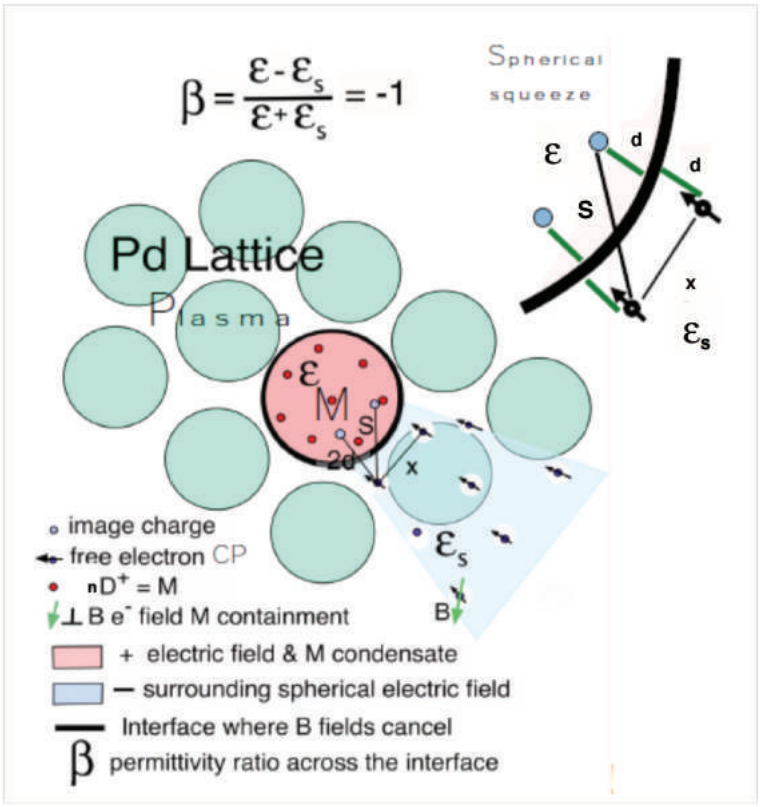

Figure 6. The interface M and CP squeeze system, accelerating e- in a D^+ E field.

Table 1. Velocities of *M'(COM)* and *alpha* in m/s

$M' = M - \alpha - E_b/c^2$kg	v_α(m/s)	$v_{M'}$ (m/s) (COM)	E_b (J)	Mom = 0 (kg/s)
3.2767×10^{-25}	33569687.1	680752.294	3.8×10^{-12}	0
1.2706×10^{-25}	33055015.2	1728709.02	3.8×10^{-12}	0
6.0184×10^{-26}	32178489.4	3552725.94	3.8×10^{-12}	0
6.6871×10^{-27}	24014821.5	23862966.6	3.8×10^{-12}	0
4.2398×10^{-29}	2699950.44	423151027	3.8×10^{-12}	0

4.7. Distribution of heat via Bremsstrahlung degradation

Each 100 ns cycle of 10^7 events melted the Pd target lattice (melting point 1825 K), as evidenced by the ejecta sites in the SEM images. As the spherical heat pulse reaches the target foil surface, an expanding hemispherical heat footprint transports heat through the Pd lattice to the circulating D_2O. The charged particles, D^+, lose their KE to the lattice via Bremsstralung cooling [4], in which high energy particles lose energy incrementally as they are bent by electromagnetic fields

With each new cycle, the molten Pd sub-surface erases the previous cycle's ejecta sites. This continuous refreshing of the Pd surface provides a new implanting surface for the next cycle's 100 ns deluge of E_b events. Within the ejecta site population there are some events that lay far enough from the nodal line to avoid the next cycle of surface heat ablation of ejecta sites. Such ejecta sites may persist for several cycles.

4.8. $2H^{++}$ Boson and M system

In 1992–1993, experiments run with H_2O showed similar target foil melting characteristics that are found in D_2O and some low calorimetry measured Q_x heating. The hope was that these experiments would serve as zero points for Q_x measurements. This was not the case, but the results were interesting. In keeping with the model, H_2O systems would produce some M condensates originating as a z-pinch implant of H_2^+. With a spin 1, H_2^+ would exhibit the bosonic character common to systems with attractive image charges. However, condensates with H^+, with a spin of $1/2$, lack the necessary bosonic character and would not compress sufficiently. This explains the lower Q_x for H_2O systems than D_2O systems. Temperature and density parameters also affect H_2^+ system in H_2O sonofusion.

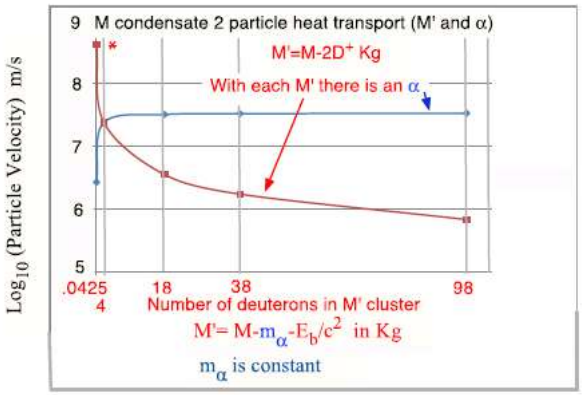

Figure 7. Velocities of COM of M' and α in m/s.M' clusters vary from 3.28 to 0.0423×10^{-27} kg or 98 to 0 D^+.

5. Conclusions

23.8 MeV, E_{b}, is the binding energy difference, B, for the α and M' event, Eq. (1). Q_x, measured calorimetrically, is equivalent to the sum of single E_{b}, 23.8 MeV, events, as surveyed from the SEM images, Fig. 1, Eq. (6).

$$\sum E_{\mathrm{b}}/\mathrm{s} = 23.8 \times 10^{13}\ \mathrm{MeV/s} = 38.2\ \mathrm{W} = Q_x \tag{6}$$

When the cavitation induced z-pinch jet implants the lattice, a charge separation occurs between free electrons and the M condensate of $n\mathrm{D}^+$. The spherical squeeze from the collective image charge of dense CPs on the interface compresses the condensate. Furthermore, this squeeze is spherically tangent to the interface, and thus acts as a magnetic containment. This picosecond pressure produces single 23.8 MeV, E_{b}, events, 10^7 events/cycle, 10^6 cycles/s, corresponding to calorimetrically measured Q_x. SEM images of target foils show clear evidence of events with temperatures reaching the Pd melting point of 1825 K, Fig. 1, [1]. Also, it can be shown that these single events conform to the Lawson Criteria [12].

In addition, the model complies with the laws of conservation of energy and momentum. These calculations, Eqs. (4) and (5), show increased velocity for M' COM with decreased number of deuterons in the M condensate. A relativistic calculation is required when the number of deuterons in the M condensate reaches 4.23×10^{-29} kg, and the system behaves like muon fusion.

The frequencies used to power piezos were changed over a span of 24 years from the initial 20–46 kHz, to the latest 1.6 MHz system. Comparisons of frequency results show that these systems have the same energy density but differ in the bubble size, number, and target foil crater production. High frequencies reduced bubble size by a factor of 1000, but the number of resonant bubbles increased by the same factor, so the energy density of ΣE_{b}, Q_x, remains the same [1]. Future development of sonofusion technology may suggest even higher frequencies, 20 MHz, which could shorten the time between 100 ns active zones, Fig. 5, to occupy a greater percentage of the MHz cycle.

Appendix

Dave Thomas, SRI Menlo Park, CA, 1991–1992, analysis used an adapted low mass, 1–6 mass units, KEV MS, to measure ^{4}He in Ar. The gas in vacuum conditions was passed through 60 g of heated CuO powder removing hydrogen. The gas passed from the bubbler to an evacuated 25 ml glass sample volume, Fig. 3. The cleansed gases were passed through a LN trap, removing Ar and D_2O, and into the MS for analysis. A possible 2 sigma value for ^{4}He was found.

Dr. Davidson, US Department of Interior, US Bureau of Mines Amarillo, TX, 1993–1994 specialized in ^{4}He MS analysis. Gas samples analyzed for ^{4}He in collected pre-treated gases as in the above SRI method returned positive results of ^{4}He at 20 ppm. The ^{4}He in the Ar supply was less than 2 ppm well below the 5 ppm that is the generally accepted value for helium in background air. ^{4}He atoms measured were 1/2 of the total atoms produced using vacuum line $pv = nRT$ [3].

In 1994, May and June, at Los Alamos National Laboratory, seven different target foil runs, gases from the bubbler filled evacuated 50 ml stainless steel sample volumes. There was no pre-treatment of the collected gases at measured pressures P_1 and then expanded to P_2 in V_2. See photo of sample volume [3]. Experiments were done using the M-2 resonator, 20 kHz. The gas samples were analyzed by Brian Oliver the at DOE ^{4}He and ^{3}He MS facilities. A report was produced, "Helium analysis of target metals", B.M. Oliver, 1995, Rockwell, International, Canoga Park, CA 91309. Analyses showed several positive results for ^{4}He and ^{3}He. Oliver used a 12 inch long $1/4$ inch diameter charcoal packed column in LN to absorb hydrogen and freeze out Ar before admission into a MS injection chamber. Using the chamber's gases, small aliquots, measuring about 5% of the chambers gas, were measured. Using the ideal gas law, several reproducible measurements were made. The total ^{4}He in resonator volume is determined from the fraction of gas collected from the free expansion of gases from resonator volume into an evacuated 50 ml valved sample volume.

Product gases, were calculated using $P_1V_1 = P_2V_2 = nkT$ to determine the ppm of ^{4}He in each aliquot delivered to the injection chamber. Three determinations were made $\pm$ 1 ppm.

This was complemented by the calorimetric measurement of 65 watts for the 19 hour run, matching the counted number of α, 552 $\pm$ 1 ppm [11]. The P_2 expansion into the sample volume contains ^{4}He in ppm that corresponds to the $Q_x E_{\mathrm{b}}$ events, Eq. (4).

Acknowledgements

I thank several individuals who helped with discussions and editing: Julie Wallace, Kim Nunlist, and Richard Spitzer.

References

[1] [1] R.S. Stringham, When bubble cavitation becomes sonofusion, *J. Condensed Matter Nucl. Sci.* **6** (2012) 1–12.
[2] Bremsstrahlung radiation http://heasarc.gsfc.nasa.gov/xstar/docs/html/node117.html
[3] R.S. Stringham, *ICCF 11 Proc.*, J. P. Biberian (Ed.) Marseilles, France, 31 Oct.–5 Nov. 2004, pp. 238–252.
[4] R.S. Stringham, Ti produces tritium that decays to helium three, *ICCF 15 Proc.*, V. Violante and F. Sarto (EDs.), Rome, Italy, 5–9 Oct. 2009, pp. 57–60. Standing wave, TiOx EDX, Tritium, 46 kHz.
[5] T.G. Leighton, *The Acoustic Bubble*, Academic Press, London, 1994, pp. 136–139.
[6] A. Bass, S. Ruuth, C. Camara, B. Merriman and S. Putterman, Molecular dynamics of extreme mass segregation in a rapidly collapsing bubble, *Phys. Rev. Lett.* **101** (2008) 234301.
[7] R.S. Stringham, Low-energy nuclear reactions sourcebook, Vol. 2, Jan Marwan and Steve Krivit (Eds.), *ACS Publications*.
[8] R.S. Stringham, The cavitation micro accelerator, *ICCF 8, Proc.*, F. Scaramuzzi (Ed.), Lerici, LaSpezia, Italy, 21–26 May 2000, pp. 299–304.
[9] N.M. Lawandy, Interaction of charged particles on surfaces, *Appl. Phy. Lett*. **95** (2009) 234101-1-3.
[10] Permittivity; un-dated explanation of http://www.princeton.edu/∼achaney/tmve/wiki100k/docs/Permittivity.html
[11] R.S. Stringham, *ICCF 17 Proc.*, S. Park and Frank Gordon (Eds.), 2012, Aug.12–17, to be published.
[12] Amasa S. Bishop, *Project Sherwood*, Addison-Wesley, 1958, pp. 12.